Microscopic description of thermal-phonon coherence: From coherent transport to diffuse interface scattering in superlattices

B. Latour, S. Volz, and Y. Chalopin[*]

Laboratoire d'Energetique Moléculaire et Macroscopique, Combustion, CNRS UPR 288, Ecole Centrale Paris,
F-92295 Chatenay-Malabry, France

We demonstrate the existence of a coherent transport of thermal energy in superlattices by introducing a microscopic definition of the phonon coherence length. A criterion is provided to distinguish the coherent transport regime from diffuse interface scattering and discuss how these can be specifically controlled by several physical parameters. Our approach provides a convenient framework for the interpretation of previous thermal conductivity measurements and calculations; it also paves the way for the design of a new class of thermal interface materials.

I. INTRODUCTION

Understanding the heat transport in condensed matter as well as at atomic interfaces is a challenging theoretical issue in solid-state physics [1,2]. Semiconductor superlattices have drawn attention for the past years for their potential applications in thermoelectricity [3], in micro- [4] and optoelectronics [1]. The thermal properties of phonon superlattices have been widely investigated numerically [5–13] and experimentally [14–19]. A phonon superlattice corresponds to a periodic arrangement of different crystalline materials. It forms a superperiod that confers a new translational symmetry to the crystal which can impact the phonon dispersion relation and subsequently the thermal transport properties in different ways.

For superlattices with perfect interfaces, it has been widely reported [5,8–15,17,19] that a minimum of the cross-plane thermal conductivity appears at a particular period thickness d_c depending on the nature of the materials. On the other hand, for superlattices with imperfect interfaces—e.g., structural interfacial defects [10–13] or pressure induced by the lattice-parameter mismatch [6,9]—the cross-plane thermal conductivity increases monotonically with the period thickness. More recently, it has been experimentally observed [18] that phonons can propagate ballistically in superlattices.

The concept of phonon coherent transport was invoked in most of these works to explain the thermal conductivity trends. However, no clear definition of the coherent transport by thermal waves has been provided so far. This concept, which is formally discussed in this paper, should not be confused with the coherence of subterahertz acoustic phonons [20,21] which have much longer wavelength than the thermal phonons and do not play a key role in thermal physics.

In this work, we first present a microscopic definition of the spatial coherence of thermal phonons and describe a method to compute the frequency-dependent spatial coherence length by tracking the fluctuations of atomic displacement

at equilibrium. To illustrate our approach, we apply this theory to argon and silicon superlattices. As a result, we explain the origin of the minimum of thermal conductivity for different period thickness which has been widely reported in the literature.

II. THEORY OF THERMAL PHONON COHERENCE

A. Definition of the spatial phonon coherence length

We first recall that any coherence phenomena can be formalized as a correlation. For instance, the spatial coherence of light is related to the spatial correlations of the electromagnetic field [22–26]; the spatial coherence of electrons also involves the spatial correlations of the electromagnetic field [27] and the spatial coherence of Bose-Einstein condensates arises from the spatial correlations of wave functions [28–30]. All those models are based on the second-order coherence theory [31].

We propose here to extend this concept to thermal phonons by postulating that the spatial phonon coherence corresponds to the spatial correlations of the atomic displacement fluctuations at equilibrium. When two atoms separated by a distance l oscillate with a given phase relationship (i.e., nonrandom), their motion is correlated. Hence, the persistence over which this correlation remains preserved at $l + \Delta l$, while increasing Δl, corresponds to the spatial phonon coherence length l_c. These spatial correlations arise from the presence of phonon wave packets in the system. Within a wave packet, atoms vibrate in phase, which means they have a correlated motion with respect to each other. Hence, the spatial coherence length $l_c(\omega)$ represents the average spatial extension of a wave packet at this frequency. As illustrated for instance in Fig. 1, all the atomic planes located at a distance less than $l_c/2$ from the reference atomic plane will exhibit motion correlations with respect to each other.

To formalize this statement, we consider the velocity field $\vec{v}\,(\vec{r}_i^{\,0\gamma}, t)$ of crystal atoms, where $\vec{r}_i^{\,0\gamma}$ corresponds to the equilibrium position of the atom γ belonging to the unit cell i. Note that the atomic displacement field $\vec{u}\,(\vec{r}_i^{\,0\gamma}, t)$ can be considered instead of the atomic velocity field, provided a factor ω^2 is added to the cross-spectral density function. The
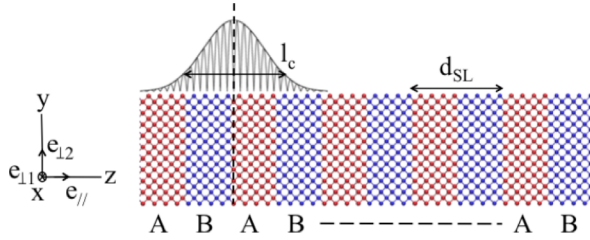
*Corresponding author: yann.chalopin@ecp.fr

FIG. 1. (Color online) Illustration of a wave packet extending on a range of atomic planes on a superlattice composed of two materials A and B. l_c corresponds to its spatial phonon coherence length. The reference plane is depicted with a dashed line.

atomic positions are decomposed as

$$\vec{r}_i^{0\gamma} = \vec{r}_i^0 + \vec{r}^\gamma, \tag{1}$$

where $\vec{r}_i^0$ stands for the position of the cell i at equilibrium and $\vec{r}^\gamma$ the position of the atom γ within the cell.

We define an orthogonal basis with $\vec{e}_\parallel$ the direction along which the correlations will be done, $\vec{e}_{\perp 1}$ and $\vec{e}_{\perp 2}$ two orthogonal vectors to $\vec{e}_\parallel$.

We introduce the mutual coherence function $\Gamma^{\alpha\beta}(|z_m - z_n|, \tau)$, with $(m,n) \in \{1, N_\parallel\}^2$, between two transverse planes of coordinates z_m and z_n along the correlation direction $\vec{e}_\parallel$:

$$\Gamma^{\alpha\beta}(z_m, z_n, \tau) = \frac{1}{k_B T\, N_\perp} \sum_{i=1}^{N_c} \sum_{j=1}^{N_c} \sum_{\gamma=1}^{N_b} \sqrt{m_i^\gamma m_j^\gamma} \langle v^\alpha(\vec{r}_i^{0\gamma}, t)\, v^\beta(\vec{r}_j^{0\gamma}, t+\tau) \rangle\, \delta\big[(\vec{r}_i^0 - \vec{r}_j^0)\cdot\vec{e}_{\perp 1}\big]\delta\big[(\vec{r}_i^0 - \vec{r}_j^0)\cdot\vec{e}_{\perp 2}\big]$$
$$\cdot\, \delta\big[\vec{r}_i^0 \cdot \vec{e}_\parallel - z_m\big]\delta\big[\vec{r}_j^0 \cdot \vec{e}_\parallel - z_n\big], \tag{2}$$

where N_c is the total number of cells in the crystal, N_b is the number of atoms in the cell basis, $N_\parallel$ is the number of cells along the direction $\vec{e}_\parallel$, $N_\perp$ is the number of cells in the orthogonal plane to $\vec{e}_\parallel$, m_i^γ is the mass of the atom γ in the cell i, k_B is the Boltzmann constant, $\delta[x]$ is the Dirac function, the superscripts α and β are two components of the vector field, and T is the system temperature which can be computed as $T = (d\, N_{\text{at}}\, k_B)^{-1} \sum_i m_i v_i^2$, with d the dimensionality of the system and N_{at} the total number of atoms in the system.

$\Gamma^{\alpha\beta}(z_m, z_n, \tau)$ is built as a sum of time correlations of velocity fields between all pairs of atoms separated by $|z_m - z_n|$. In the triple sum, the atoms i and j belong respectively to the atomic plane located at z_m and z_n. Taking the Fourier transform of Eq. (2) allows us to extract the two-point cross-spectral density function $W^{\alpha\beta}(z_m, z_n, \omega)$. For each frequency of the phonon spectrum, $W^{\alpha\beta}(z_m, z_n, \omega)$ contains the space-dependent correlation along the direction $\vec{e}_\parallel$. The superscripts α and β are removed to simplify the notation.

The degree of coherence $\mu(z_m, z_n, \omega)$ is then calculated from the two-point cross-correlation function as

$$\mu(z_m, z_n, \omega) = \frac{W(z_m, z_n, \omega)}{[W(z_m, z_m, \omega)]^{1/2}\, [W(z_n, z_n, \omega)]^{1/2}}. \tag{3}$$

Note that $W(z_m, z_m, \omega)$ corresponds to the local density of states of all atoms present at $z = z_m$ and thus is a real number. $\mu(z_m, z_m, \omega)$ contains the two-point correlation of all possible pairs of planes. From it, we can now define the spatial cross correlation, noted $C(k\Delta z, \omega)$, as

$$C(k\Delta z, \omega) = \frac{1}{N_\parallel - k} \sum_{i=1}^{N_\parallel - k} \mu(z_i, z_{i+k-1}, \omega) \tag{4}$$

with $k \in \{0 \ldots N_\parallel - 1\}$ and Δz the spatial resolution of the correlation. If $\vec{e}_\parallel$ is collinear to one of the lattice vectors, Δz corresponds to the lattice parameter along this direction.

The spatial coherence length is defined as the spatial decay of the cross-correlation function $C(k\Delta z, \omega)$. Therefore, we can extract the spatial phonon coherence length $l_c(\omega)$ from the variance of the normalized cross-spectral density function

[29,30] as

$$l_c^2(\omega) = \frac{\sum_{k=0}^{N_\parallel - 1} |C(k\Delta z, \omega)|^2 (k\Delta z)^2}{\sum_{k=0}^{N_\parallel - 1} |C(k\Delta z, \omega)|^2}$$
$$- \left(\frac{\sum_{k=0}^{N_\parallel - 1} |C(k\Delta z, \omega)|^2 k\Delta z}{\sum_{k=0}^{N_\parallel - 1} |C(k\Delta z, \omega)|^2} \right)^2. \tag{5}$$

The normalized cross-spectral density function plays here the role of a density probability function. However, this estimator of the variance is convenient for analytical problems but too sensitive to noise for numerical simulations.

We define now another estimator based on the cumulative distribution function $F(n\Delta z, \omega)$ of the normalized cross-spectral density:

$$F(n\Delta z, \omega) = \frac{\sum_{k=0}^{n} |C(k\Delta z, \omega)|^2}{\sum_{k=0}^{N_\parallel - 1} |C(k\Delta z, \omega)|^2} \tag{6}$$

with $n \in \{0 \ldots N_\parallel - 1\}$.

As a cumulative distribution function, $F(n\Delta z, \omega)$ is bounded between 0 and 1. We estimate here the spatial phonon coherence length $l_c(\omega)$ as the distance for which the cumulative distribution function is equal to 95%. In other words, at the coherence length, 95% of the total correlated signal is taken into account.

B. Definition of coherent and incoherent phonon transport in superlattices

We introduce the characteristic dimensionless number $l_c(\omega)/d_{\text{SL}}$ to determine the phonon transport regime.

When $l_c(\omega) \geqslant d_{\text{SL}}$, the transport of phonon modes at this frequency is said to be coherent because the spatial extension of the corresponding wave packet is greater than the period thickness. It travels in a new homogeneous material, free of interfaces, with a dispersion relation governed by zone folding effects of the superlattice. The mean free path is not impacted by interface scattering. Hence, for high mean free

path materials, as long as the period remains smaller than $l_c(\omega)$, the phonon propagates ballistically as has been experimentally observed in GaAs/AlAs superlattices [18].

On the contrary, when $l_c(\omega) \leqslant d_{SL}$, the transport becomes incoherent. The spatial extension of the wave packet is smaller than the period thickness, so phonons undergo diffuse interface scattering. In this regime the mean free path is bounded by the period thickness of the superlattice.

III. COMPUTATION OF THE SPATIAL PHONON COHERENCE LENGTH FROM EQUILIBRIUM MOLECULAR DYNAMICS SIMULATIONS

To compute the cross-spectral density function and so the spatial phonon coherence length, the statistical fluctuations of the velocity field $\vec{v}\,(\vec{r}_i^{\,0\gamma}, t)$ have to be captured at thermal equilibrium. This can be done with equilibrium molecular dynamics simulations.

A. Spatial coherence in argon superlattices

We have first modeled argon superlattices, because it has a short phonon mean free path [9]. We have employed a Lennard-Jones (LJ) potential at 40 K. The interatomic potential between atoms of two different layers has been set following an arithmetic mean [8]. The first layer is composed of argon atoms interacting according to a LJ potential with a depth twice larger than the one of normal argon [32]. In the second layer, the LJ depth is 2.5 larger than in the first one. Periodic boundary conditions have been applied along the interface cross section (2.5×2.5 nm^2). The size of the system is then fixed to 80 nm to prevent size effects from the calculation of the coherence length. The superlattices have been relaxed in the NPT ensemble for 2 ns. The time step is fixed at $\delta t = 1$ fs. Equilibrium trajectories of 250 ps with an ensemble average on ten simulations in the NVE ensemble are considered to compute the cross-spectral density function.

The local density of states (LDOS) is first computed in the microcanonical ensemble for various layer thickness, by calculating the trace of the cross-spectral density function $W(|z_m - z_n|, \omega)$. Results are depicted in Figs. 2(a) and 2(c). As d_{SL} increases, a clear evidence of the phonon band folding is observed below $d_{SL} = 4$ nm. Above 4 nm, the phonon LDOS no longer depends on d_{SL}.

The corresponding phonon coherence lengths are also presented in Figs. 2(b) and 2(d), only for longitudinal phonons (along $\vec{e}_{\parallel}$). The transverse phonon case will be discussed later. The correlation direction $\vec{e}_{\parallel}$ is along (001). For $d_{SL} \leqslant 4$ nm, l_c decreases when d_{SL} increases, while it becomes independent from d_{SL} for larger period thickness. As low-frequency phonons have a large wavelength, their spatial coherence length should be greater than the high-frequency ones, which is consistent with Figs. 2(b) and 2(d).

The quantity $\log_{10}[l_c(\omega)/d_{SL}]$ is depicted in Fig. 3 to compare the spatial coherence length to the period thickness and so to determine the phonon transport regime. For $d_{SL} \leqslant 4$ nm, $l_c(\omega) \geqslant d_{SL}$, the phonon transport is mainly coherent. The thermal transport is governed by the propagation of wave packets which do not scatter at the interfaces. In Fig. 2(a), we observe a clear signature of the folding of the
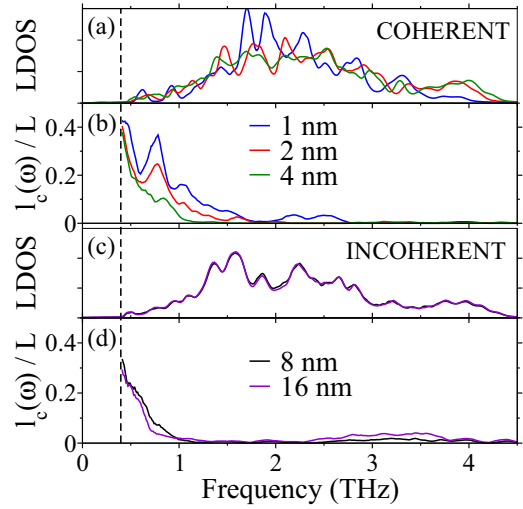

FIG. 2. (Color online) (a) The LDOS for d_{SL} from 1 to 4 nm; (b) spatial phonon coherence length normalized by the system length for $d_{SL} = 1$, 2, and 4 nm; (c) the LDOS for d_{SL} for 8 and 16 nm; (d) spatial phonon coherence length normalized by the system length for $d_{SL} = 8$ and 16 nm.

Brillouin zone at various period thickness. For $d_{SL} > 4$ nm, the spatial coherence length of the dominant phonon frequencies has the same order of magnitude or is smaller than d_{SL}. The phonon transport is no longer prescribed by zone folding effects which are consistently observed in the LDOS calculation. Interestingly, 4 nm coincides with the critical thickness d_c at which the trend of the thermal conductivity of this superlattice reverses as reported earlier [9].

Previous results were obtained for a fixed system length L. Size effect on the phonon coherence length is now investigated
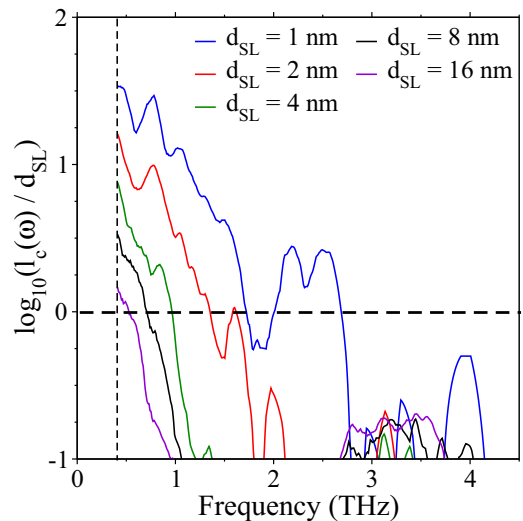

FIG. 3. (Color online) $\log_{10}[l_c(\omega)/d_{SL}]$ is calculated to determine the phonon transport regime. When $\log_{10}[l_c(\omega)/d_{SL}] > 0$ (respectively < 0), the phonon transport is coherent (respectively incoherent), the wave-packet spatial extension is larger (respectively smaller) than d_{SL}. The horizontal dotted line indicates the threshold between the coherent and the incoherent regime.
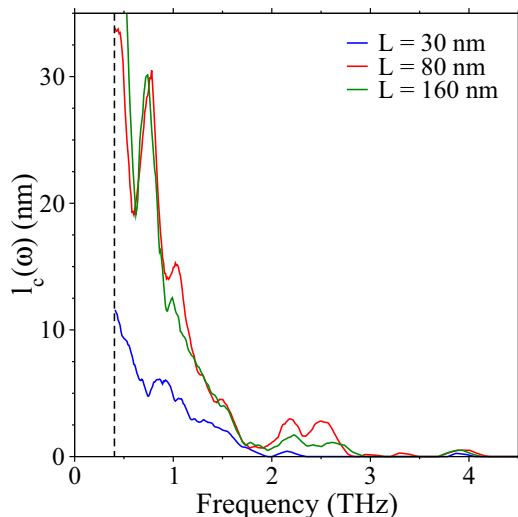
FIG. 4. (Color online) Effect of the system size on argon super-lattices in the coherent regime with $d_{SL} = 1$ nm.

on argon superlattices in both coherent and incoherent regimes. Figure 4 shows the impact of the number of periods—i.e., of the total length of the superlattice—with $d_{SL} = 1$ nm. The coherence length clearly depends on the system length between $L = 30$ nm and 80 nm, especially for frequencies lower than 2 THz. Then, a saturation appears at 80 nm so the coherence length spectrum does not change for larger total length. The size-effect study was also carried out in the incoherent regime for argon superlattices with $d_{SL} = 16$ nm. In Fig. 5, the phonon coherence spectrum is independent of the system length in the incoherent regime. Knowing that the coherence length corresponds to the spatial extension of the wave packets, when the wave packets are greater than the period thickness, they can interact to construct a larger wave packet. Hence, coherence properties depend on the number of unit cells in the system. Of course, the coherence length for the case of coherent transport will saturate for superlattice length much
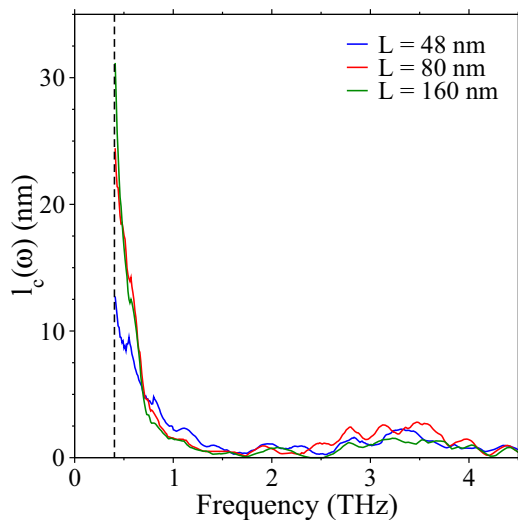
larger than the dominant phonon mean free path, as umklapp processes will destroy coherence properties. On the contrary, in the incoherent regime, the coherence length will reach a limit when the period thickness is much larger than the mean free path of each intrinsic material of the superlattice.

B. Spatial coherence in silicon superlattices

We now turn to a more realistic system made of silicon. In addition to its technological interests [33], the dominant mean free path Λ in bulk silicon is larger than the system length L simulated in this paper, contrary to argon superlattices. In this study, the Stillinger-Weber potential [34] has been considered. To avoid any pressure effect at the interfaces, we have built superlattices of silicon and heavy silicon (hSi) atoms with a mass mismatch $m_{hSi} = 2m_{Si}$ to create an acoustic impedance mismatch close to the one of real Si/Ge superlattices. The same simulation parameters than for argon superlattices have been used to extract the equilibrium trajectories.

The effect of the period thickness d_{SL} is first investigated at 300 K on both longitudinal (along $\vec{e}_{\parallel}$) and transverse (along $\vec{e}_{\perp 1}$ and $\vec{e}_{\perp 2}$) components of the velocity field. The length of superlattices is fixed to 40 nm to avoid any size effect when changing d_{SL}. The quantity $\log_{10}[l_c(\omega)/d_{SL}]$ is plotted in Fig. 6. No significant difference between longitudinal and transverse phonons is observed. For the sake of clarity, all the following considerations are developed for longitudinal phonons but can be generalized for transverse ones. As d_{SL} increases, l_c decreases up to 80% between $d_{SL} = 1$ and 8 nm. Moreover, the optical-phonon wave packets have a short coherence length, even for the small period.

Size-effect investigations are carried out to unveil the effect of the system size L on the spatial phonon coherence length $l_c(\omega)$ for Si/hSi superlattices with d_{SL} equal to 1 and 8 nm. Figure 7 compares the coherence length for L from 20 to
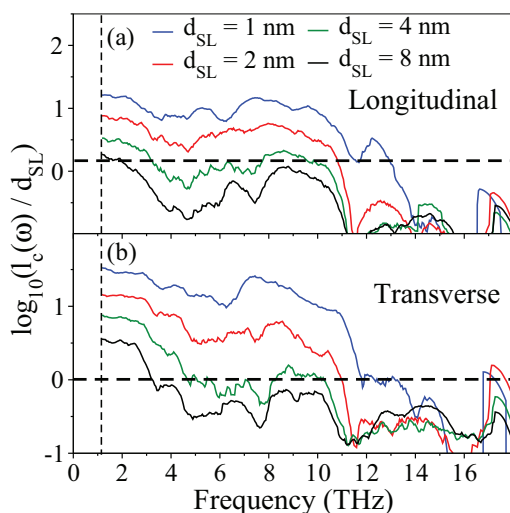

FIG. 6. (Color online) (a) $\log_{10}[l_c(\omega)/d_{SL}]$ for the longitudinal component of the velocity field for Si/hSi superlattices with period thickness ranging 1–8 nm. (b) $\log_{10}[l_c(\omega)/d_{SL}]$ for the transverse components of the velocity field for Si/hSi superlattices with period thickness ranging 1–8 nm. Coherent transport is observed below $d_{SL} = 4$ nm.

FIG. 5. (Color online) Effect of the system size on argon super-lattices in the incoherent regime with $d_{SL} = 16$ nm.
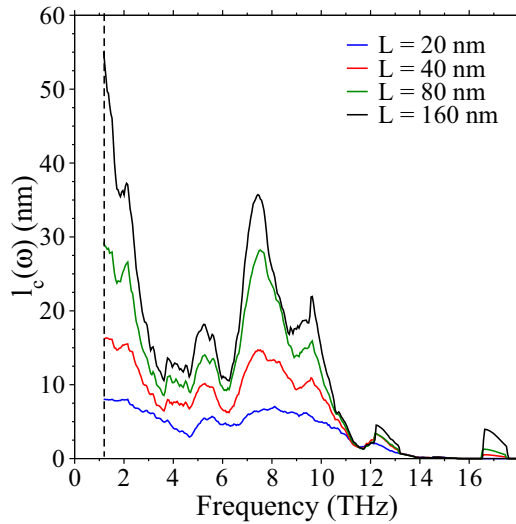
FIG. 7. (Color online) Effect of the system size on Si/hSi superlattices with $d_{SL} = 1$ nm.

160 nm in the coherent regime. The size effect is similar to the one observed on argon superlattices in the coherent regime. However, even at 160 nm, the coherence length spectrum does not completely saturate.

In Fig. 8, two features of convergence can be extracted for silicon superlattices with $d_{SL} = 8$ nm. For frequencies lower than 4 THz, the coherence length does not show any saturation until $L = 160$ nm. This is due to phonons that have larger wavelength. For higher frequencies, a clear saturation of the coherence length is observed at $L = 80$ nm.

The temperature effect is next investigated on the superlattice with the highest coherence properties, e.g., $d_{SL} = 1$ nm and $L = 40$ nm. The corresponding l_c is plotted in Fig. 9 for temperature ranging 300–1000 K. Increasing the temperature dramatically alters the coherence properties with a reduction of l_c up to 70% between 300 and 1000 K for optical
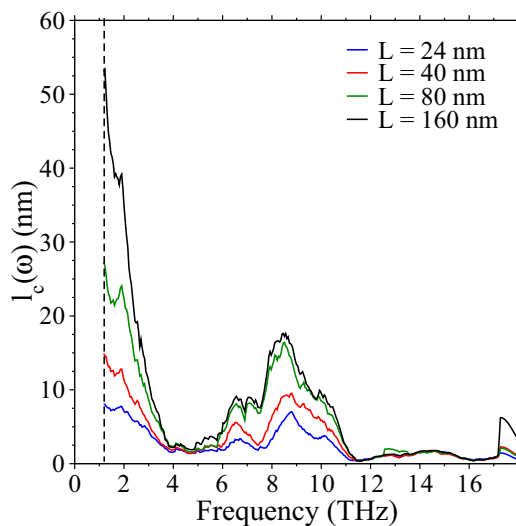

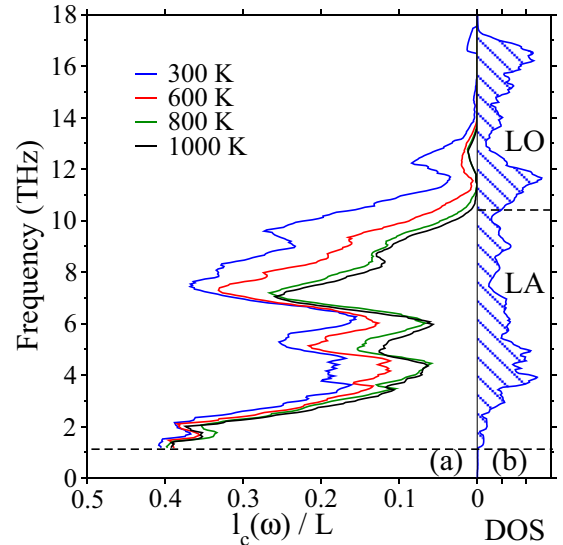FIG. 8. (Color online) Effect of the system size on Si/hSi superlattices with $d_{SL} = 8$ nm.

FIG. 9. (Color online) (a) Spatial phonon coherence length $l_c(\omega)$ normalized by the system length L for silicon superlattices with $d_{SL} = 1$ nm, for $T = 300, 600, 800,$ and 1000 K. (b) Phonon DOS of the silicon superlattice with $d_{SL} = 1$ nm at 300 K.

frequencies due to anharmonic scattering. The coherence of the low-frequency phonons remains very hard to affect.

To investigate how the coherence length can be further reduced, we have considered interfacial mixing in a Si/hSi superlattice with $d_{SL} = 2$ nm. For each period of the superlattice, N atomic planes at each side of the Si/hSi interface are modified by exchanging randomly the nature of atoms at a certain percentage m. Three configurations have been compared on Fig. 10(a): perfect interfaces, and where interfaces includes 10% and 50% of mixing on only the first contact plane. For frequencies lower than 4 THz, coherence lengths remain weakly damaged by the defected interfaces, as phonons have larger wavelength than the interface roughness. However, coherence is more affected than for the case of high temperature. For higher frequencies, l_c decreases dramatically. When considering 50% mixing, the coherence length breaks down for frequencies above 4 THz. An important aspect of this study reveals that this effect occurs with a very small fraction of defect atoms (∼1%) compared to the total number of atoms.

Figure 10(b) further illustrates how the mixing expanded on several atomic planes [33] destroys the coherence properties for $d_{SL} = 2$ nm with only 10% of interfacial mixing. Note that introducing an interfacial mixing over four atomic planes corresponds to an alloy for this superlattice. When increasing the number of atomic planes N with mixing, $l_c(\omega)$ decreases dramatically up to two orders of magnitude when N goes from 1 to 3 for frequencies larger than 4 THz. Therefore, invoking coherence effects in superlattices where deep interfacial mixing occurs remains only valid for phonons with a frequency below 4 THz; otherwise, interfaces are purely diffuse. In addition, it also demonstrates that part of the phonons are still in a coherent regime in alloy systems.

To corroborate our results of coherence to thermal transport properties, we have computed the cross-plane thermal conductivity κ of the Si/hSi superlattices with a Green-Kubo
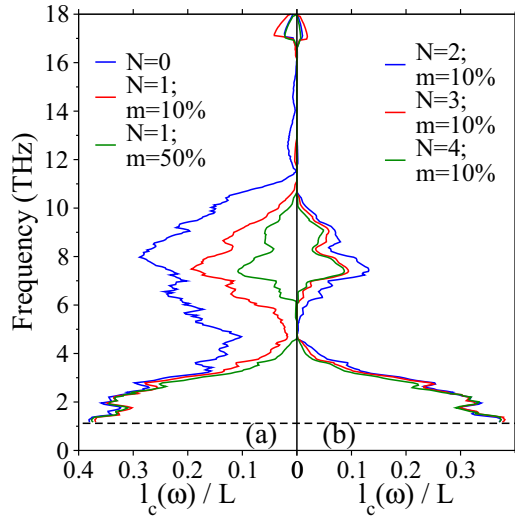
FIG. 10. (Color online) (a) Spatial phonon coherence length $l_c(\omega)$ normalized by the system length L for Si/hSi superlattices with $d_{SL} = 2$ nm for perfect interfaces ($N = 0$), then 10% ($N = 1$; $m = 10\%$) and 50% ($N = 1$; $m = 50\%$) interfacial mixing on 1 atomic layer away from each interface. (b) Spatial phonon coherence length $l_c(\omega)$ normalized by the system length L for Si/hSi superlattices with $d_{SL} = 2$ nm for perfect interfaces ($N = 0$), then 10% ($m = 10\%$) interfacial mixing on N atomic layers away from each interface, where $N \in \{1,4\}$.

approach [35,36] at 500 K. It is illustrated for the case of perfect interfaces in Fig. 11.

The minimum of thermal conductivity is recovered for $d_c = 4$ nm. Below d_c, the thermal conductivity decreases while increasing the period thickness d_{SL} due to phonon band folding. Above d_c, as the phonon transport is incoherent, interface scattering occurs and the effective interface conductance becomes independent from d_{SL}. It confirms the transition from a coherent to an incoherent regime predicted
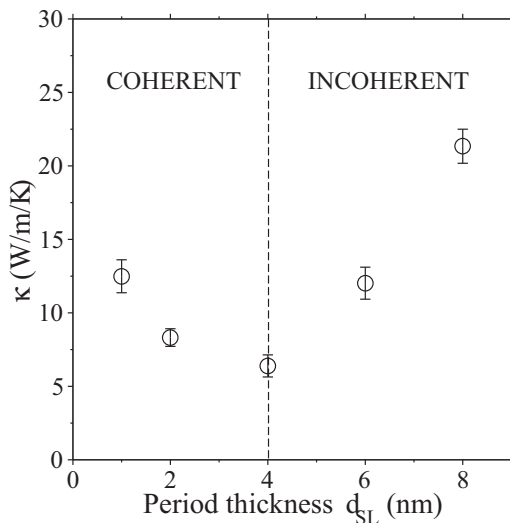

FIG. 11. The cross-plane thermal conductivity κ for perfect Si/hSi superlattices at 500 K from Green-Kubo calculations.

by Fig. 6. This value $d_{SL} = 4$ nm is also consistent with previous experiments on strained Si/Ge superlattices [14,15]. In addition, the transition occurs at the same period as for the previous argon superlattices. Experiments on Si/Ge superlattices [14,15], on Bi_2Te_3/Sb_2Te_3 superlattices [16], on (Zr,W)N/ScN superlattices [17], and on perovskite oxide $SrTiO_3/CaTiO_3$ and $SrTiO_3/BaTiO_3$ superlattices [19] also showed a transition for the same range of period thickness despite the different nature of materials.

C. Summary of phonon transport in superlattices

We have seen in the previous sections that many characteristic lengths are involved in the phonon transport in superlattices. Heat is carried by a wide spectrum of phonon wave packets, with different transport regimes depending on the magnitude of the characteristic lengths. Each normal mode has a specific frequency ν, wavelength λ, and wave vector $\vec{k} = 2\pi/\lambda\,\vec{u}$, where $\vec{u}$ is the unit vector indicating the propagation direction. What follows is developed for a unique normal mode $\nu(\vec{k})$ but should be extended to the whole spectrum when considering the thermal properties of superlattices. Each wave packet has a finite spatial extension, defined as the spatial coherence length l_c. As it is depicted in Fig. 12, the coherence length is always larger than the associated wavelength. The wave packet has a mean free path Λ_{bulk1} (respectively Λ_{bulk2}) in the bulk material 1 (respectively 2), which are the two materials composing the superlattice. For simplicity, we assume $\Lambda_{bulk1} \approx \Lambda_{bulk2}$ and we note $\Lambda_{bulk1,2}$ the average value. The mean free path of the wave packet in the superlattice Λ_{SL} may differ from $\Lambda_{bulk1,2}$. Finally, the period thickness d_{SL} and the system length L characterize the superlattice geometry.

The two main characteristic lengths, which determine the transport regime of the phonon wave packet in the superlattice, are the phonon coherence length l_c and the mean free path in bulk materials $\Lambda_{bulk1,2}$. The comparison between l_c and the period thickness d_{SL} indicates if the transport is coherent or not in the superlattice. $\Lambda_{bulk1,2}$ is compared to d_{SL} and also to L to see if the transport could be ballistic or not in the superlattice. These analyses lead to six potential transport regimes, depicted in Fig. 12. For each case is given a schematic trend of the cross-plane thermal conductivity, first as a function of d_{SL} for a constant L, then with respect to L for a constant d_{SL}.

Case (a). The coherence length l_c is greater than d_{SL} and the bulk mean free path $\Lambda_{bulk1,2}$ is larger than the superlattice length L. The spatial extension of the phonon wave packet is larger than the period thickness: it is created from the normal modes of the folded Brillouin zone. Therefore, the larger the period thickness, the more folded is the phonon dispersion, opening more and more band gaps. It might lead to a lower group velocity so to a smaller thermal conductivity. It travels in an effective homogeneous medium, free of interfaces in a ballistic regime, as $\Lambda_{bulk1,2} > L$. The mean free path Λ_{SL} is thus bounded by the superlattice length L, $\Lambda_{SL} = L$. As a consequence, the thermal conductivity exhibits a increasing trend when making L larger [18].

Case (b). The coherence length l_c is smaller than d_{SL} and the bulk mean free path $\Lambda_{bulk1,2}$ is greater than the superlattice length L. The phonon wave packet is located in only one layer material so it cannot feel the superlattice periodicity. The
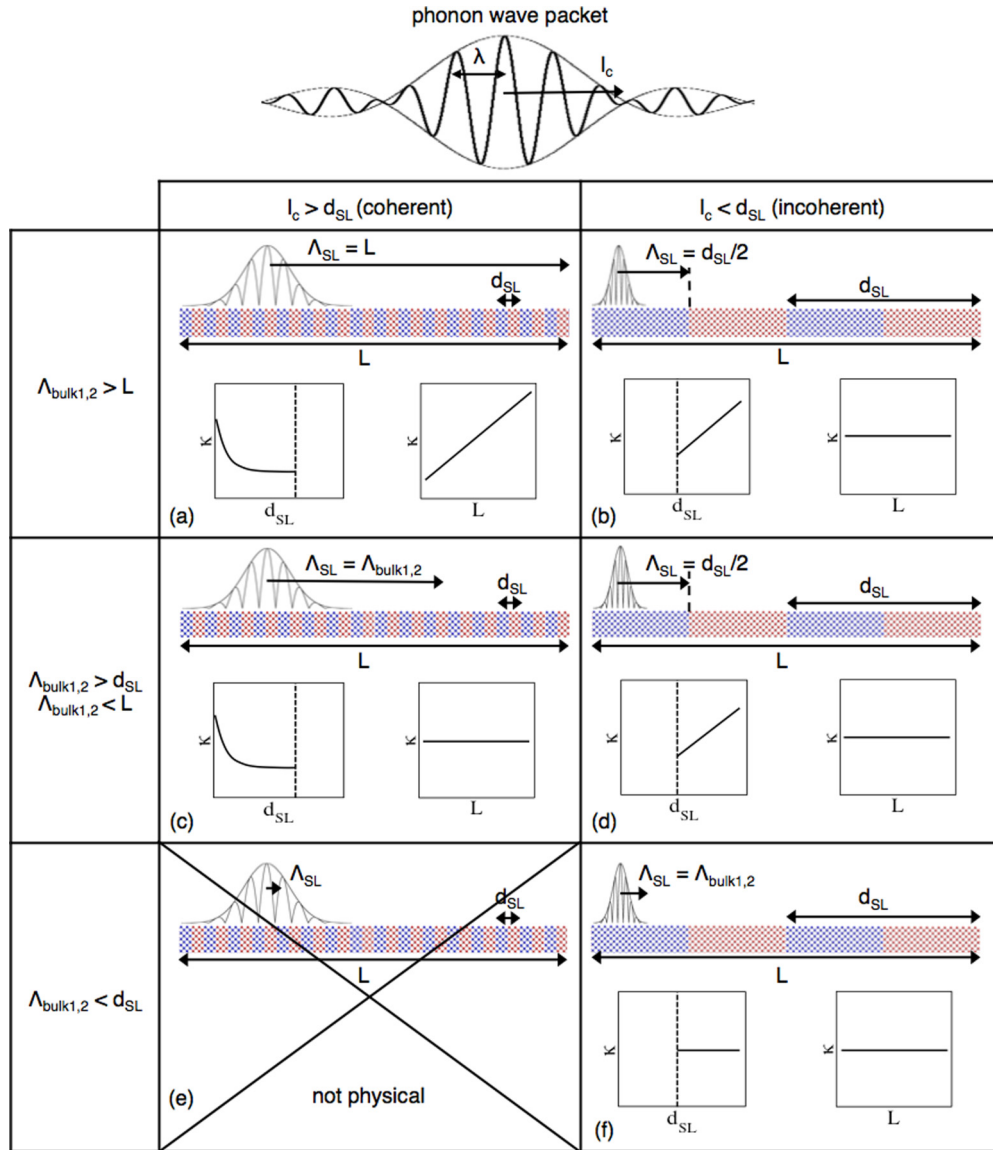
FIG. 12. (Color online) Schematic representation of all phonon characteristic lengths that are involved in the phonon transport in superlattices. l_c is the phonon coherence length, λ is the wavelength associated to the wave packet, d_{SL} is the period thickness of the superlattice, and L is its length. For simplification, the two bulk materials 1 and 2 are assumed to have a similar mean free path, noted $\Lambda_{bulk1,2}$. Finally, Λ_{SL} represents the mean free path of the wave packet in the superlattice. For each of these six cases, two trends for the thermal conductivity κ are depicted: one as a function of the period thickness d_{SL} with a constant length L and one with respect to L with a constant d_{SL}.

phonon dispersion corresponds to the bulk dispersion relations of material 1 or 2, depending on which layer it is. Therefore, its group velocity is independent from d_{SL}. Even if $\Lambda_{bulk1,2}$ is greater than L, the wave packet scatters at the interfaces, limiting the mean free path in the superlattice Λ_{SL} to half of the period thickness. As a consequence, the thermal conductivity is higher when the distance between the interfaces increases and is not sensitive to L.

Case (c). Like in case (a), the coherence length is greater than d_{SL}, so the phonon transport is still coherent and governed by band folding. As a consequence, the thermal conductivity decreases when increasing d_{SL}. Here, the bulk phonon mean free path is smaller than the system length but greater than d_{SL}. As the wave packet is not sensitive to the interface

scattering, the mean free path in the superlattice Λ_{SL} has the same order of magnitude as in the bulk material. So, the thermal conductivity does not depend on the system length, as the superlattice is large enough to have phonon-phonon interactions.

Case (d). It is identical to case (b). The transport is incoherent and the interface scattering still limits the phonon mean free path in the superlattice, $\Lambda_{SL} = d_{SL}$. So, the thermal conductivity increases with respect to d_{SL} and is insensitive to L.

Case (e). The phonon coherence length should be always smaller than the bulk phonon mean free path. Indeed, considering a wave packet, which cannot propagate on a distance equal to its spatial extension without scattering, is not physical.

Case (f). When the coherence length and the bulk mean free path are smaller than the period thickness, the wave packet is located in only one material layer and encounters many phonon-phonon collisions before scattering at the interfaces. So the thermal properties of the superlattice correspond to an average of the two bulk materials with the addition of the interface resistance between them. κ is thus independent from d_{SL} and L.

Interestingly, when the phonon transport is coherent [cases (a) and (c)], it is always associated with a ballistic transport, meaning $\Lambda_{SL} > d_{SL}$. In another word, the observed ballistic transport in superlattices is a consequence of the fact that the coherence length of phonon wave packets is larger than the period d_{SL}.

All phonon modes contribute to the total thermal properties of the superlattice, each one with its own phonon transport regime. When considering the evolution of the thermal conductivity with d_{SL}, the transition from a coherent ballistic regime [case (a) or (c)] to interface scattering regime [case (b) or (d)] is different for each normal mode. Consequently, the minimum of thermal conductivity is obtained when most of the acoustic phonons undergo interface scattering. Finally, we wish to recall that this minimum is related to the anharmonicity of the crystal. Indeed, if one considers a harmonic system, the coherence length should be infinite and no transition to an incoherent regime could be observed.

IV. CONCLUSION

In this paper, we have defined the coherence of thermal phonons at the nanoscale by introducing a microscopic theory of the phonon spatial coherence length $l_c(\omega)$. This length can be assessed from the spatial correlation of the atomic motion in the crystal. We have introduced the characteristic dimensionless number $l_c(\omega)/d_{SL}$ which allows us to predict the switch from a coherent to diffuse interface transport regime. It generally explains the thermal conductivity trend of superlattices widely reported so far in the literature, which exhibits a transition from a coherent to diffuse interface transport identified by a minimum in the conductivity trend. Moreover, this method can help to quantitatively predict the minimum of thermal conductivity as several phonon transport regimes are involved in superlattices.

ACKNOWLEDGMENT

[1] D. G. Cahill, W. K. Ford, K. E. Goodson, G. D. Mahan, A. Majumdar, H. J. Maris, R. Merlin, and S. R. Phillpot, J. Appl. Phys. **93**, 793 (2003).

[2] V. P. Carey, G. Chen, C. Grigoropoulos, M. Kaviany, and A. Majumdar, Nanoscale Microscale Thermophys. Eng. **12**, 1 (2008).

[3] A. Shakouri, Annu. Rev. Mater. Sci. **41**, 399 (2011).

[4] E. Pop, Nano Res. **3**, 147 (2010).

[5] M. V. Simkin and G. D. Mahan, Phys. Rev. Lett. **84**, 927 (2000).

[6] Y. Chalopin, K. Esfarjani, A. Henry, S. Volz, and G. Chen, Phys. Rev. B **85**, 195302 (2012).

[7] I. Savić, D. Donadio, F. Gygi, and G. Galli, Appl. Phys. Lett. **102**, 073113 (2013).

[8] S. Volz, J. B. Saulnier, G. Chen, and P. Beauchamp, Microelectron. J. **31**, 815 (2000).

[9] Y. Chen, D. Li, J. R. Lukes, Z. Ni, and M. Chen, Phys. Rev. B **72**, 174302 (2005).

[10] B. C. Daly, H. J. Maris, K. Imamura, and S. Tamura, Phys. Rev. B **66**, 024301 (2002).

[11] K. Imamura, Y. Tanaka, N. Nishiguchi, S. Tamura, and H. J. Maris, J. Phys.: Condens. Matter **15**, 8679 (2003).

[12] K. Termentzidis, P. Chantrenne, J. Y. Duquesne, and A. Saci, J. Phys.: Condens. Matter. **22**, 475001 (2010).

[13] E. S. Landry and A. J. H. McGaughey, Phys. Rev. B **79**, 075316 (2009).

[14] T. Borca-Tasciuc, W. Liu, J. L. Liu, T. Zeng, D. W. Song, C. D. Moore, G. Chen, K. L. Wang, M. S. Goorsky, T. Radetic, R. Gronsky, T. Koga, and M. S. Dresselhaus, Superlattices Microstruct. **28**, 199 (2000).

[15] S. Chakraborty, C. A. Kleint, A. Heinrich, C. M. Schneider, J. Schumann, M. Falke, and S. Teichert, Appl. Phys. Lett. **83**, 4184 (2003).

[16] R. Venkatasubramanian, Phys. Rev. B **61**, 3091 (2000).

[17] V. Rawat, Y. K. Koh, D. G. Cahill, and T. D. Sands, J. Appl. Phys. **105**, 024909 (2009).

[18] M. N. Luckyanova, J. Garg, K. Esfarjani, A. Jandl, M. T. Bulsara, A. J. Schmidt, A. J. Minnich, S. Chen, M. S. Dresselhaus, Z. Ren, E. A. Fitzgerald, and G. Chen, Science **338**, 936 (2012).

[19] J. Ravichandran, A. K. Yadav, R. Cheaito, P. B. Rossen, A. Soukiassian, S. J. Suresha, J. C. Duda, B. M. Foley, C. Lee, Y. Zhu, A. W. Lichtenberger, J. E. Moore, D. A. Muller, D. G. Schlom, P. E. Hopkins, A. Majumdar, R. Ramesh, and M. A. Zurbuchen, Nat. Mater. **13**, 168 (2014).

[20] A. Huynh, B. Perrin, B. Jusserand, and A. Lemaitre, Appl. Phys. Lett. **99**, 191908 (2011).

[21] Y. Ezzahri, S. Grauby, J. M. Rampnoux, H. Michel, G. Pernot, W. Claeys, S. Dilhaire, C. Rossignol, G. Zeng, and A. Shakouri, Phys. Rev. B **75**, 195309 (2007).

[22] E. Wolf, J. Opt. Soc. Am. **72**, 343 (1982).

[23] E. Wolf, J. Opt. Soc. Am. A **3**, 76 (1986).

[24] R. Carminati and J.-J. Greffet, Phys. Rev. Lett. **82**, 1660 (1999).

[25] F. Marquier, K. Joulain, J. P. Mulet, R. Carminati, J. J. Greffet, and Y. Chen, Phys. Rev. B **69**, 155412 (2004).

[26] J. Tervo, T. Setala, and A. T. Friberg, J. Opt. Soc. Am. A **21**, 2205 (2004).

[27] A. Singer, I. A. Vartnyants, M. Kuhlmann, S. Duesterer, R. Treusch, and J. Feldhaus, Phys. Rev. Lett. **101**, 254801 (2008).

[28] G. H. S. Franke-Arnold and S. M. Barnett, J. Phys. B **34**, 945 (2001).

[29] S. M. Barnett, S. Franke-Arnold, A. S. Arnold, and C. Baxter, J. Phys. B **33**, 4177 (2000).

[30] A. Bezett, E. Toth, and P. B. Blakie, Phys. Rev. A **77**, 023602 (2008).

[31] L. Mandel and E. Wolf, *Optical Coherence and Quantum Optics* (Cambridge University Press, New York, 1995).

[32] A. Michels, H. Wijker, and H. K. Wijker Physica **15**, 627 (1949).

[33] K. Lyutovich and E. Kasper, *Properties of Silicon Germanium and SiGe:Carbon* (Inspec, IEE, London, 2000).

[34] F. H. Stillinger and T. A. Weber, Phys. Rev. B **31**, 5262 (1985).

[35] R. Kubo, M. Toda, and N. Hashitsume, *Statistical Physics II* (Springer-Verlag, Berlin, 1985).

[36] M. P. Allen and D. J. Tildesley, *Computer Simulation of Liquids* (Clarendon, Oxford, 1987).